International Journal of Electrochemical Science 20 (2025) 101090

Contents lists available at ScienceDirect

International Journal of Electrochemical Science

journal homepage: www.editorialmanager.com/ijoes

In-operando 3D visualization of nickel electrodeposition and mass transport phenomena: Insights from X-ray microcomputed tomography

Rodrigo F.B. de Souza, Andrea S. Del Pozzo, Antonio D. Giuliano, Gabriel Silvestrin, Lorenzo De Micheli, Edson P. Soares, Claudia Giovedi, Luis A.A. Terremoto, Samir L. Somessari, Almir O. Neto *, Wilson Calvo

Instituto de Pesquisas Energéticas e Nucleares, IPEN/CNEN-SP, Av. Prof. Lineu Prestes, 2242 Cidade Universitária,, São Paulo, SP CEP 05508-000, Brazil

ARTICLE INFO

Keywords:
Electrodeposition
Nickel
X-ray Micro-computed Tomography
Mass Transport
Electrochemical Imaging
Ionic Migration

ABSTRACT

Nickel electrodeposition is widely used in industrial applications due to its ability to enhance the mechanical and corrosion resistance of metallic substrates. However, understanding mass transport mechanisms during electrodeposition remains a challenge, as conventional models struggle to describe complex three-dimensional phenomena such as concentration gradients, depletion zones, and convective instabilities. In this study, we employ X-ray micro-computed tomography (X-ray μCT) *in-operando* imaging technique to investigate the electrodeposition of nickel on titanium under potentiostatic conditions. Chronoamperometric analysis and scanning electron microscopy (SEM) confirmed distinct deposition behaviors at −0.5 V and −1.2 V, with negligible deposition at the lower potential and significant nickel growth, including dendritic structures, at the higher potential. The X-ray μCT images revealed the formation of structured ionic layers near the electrode surfaces, with Ni^{2+} ion migration and concentration gradients influencing deposition dynamics. At −1.2 V, depletion zones and convective instabilities were identified, suggesting a competition between diffusion, migration, and Rayleigh-Bénard convection. These findings demonstrate the feasibility of X-ray μCT for real-time 3D visualization of electrochemical processes, providing novel insights into mass transport during electrodeposition.

1. Introduction

Electrodeposition is one of the most versatile and technologically relevant electrochemical processes today, with both decorative and engineering applications [1]. It enables the production of metallic coatings with anticorrosive properties, electrical conductivity, mechanical strength, and distinct aesthetic characteristics [2]. In particular, nickel electrodeposition provides a coating that significantly enhances the corrosion resistance and mechanical properties of steels, making it widely used in industrial applications [2]. Over the past decades, advances in the understanding of deposition mechanisms, optimization of operational parameters, and the development of hybrid metallic alloys have expanded the industrial applications of this process [3].

Despite significant technological advancements in the field, a detailed study of mass transport during electrodeposition remains a challenge. While transport equations already account for phenomena such as migration, convection, and diffusion, extending these parameters to three dimensions results in highly complex structures [4]. Additionally, secondary effectssuch as Rayleigh-Bénard convection [5], mass transfer correlations forlaminar and turbulent flow [6] and other intricate transport phenomenafurther complicate the modeling process [2,7].

Several efforts have been made to understand and simulate these processes [3,8,9], but there is considerable difficulty in directly observing these effects experimentally, especially in real-time and in three dimensions. A technique capable of addressing this gap would greatly benefit both experimental and theoretical studies in this field.

In this context, X-ray microcomputed tomography (X-ray μCT) emerges as a promising technique, as it enables non-destructive three-dimensional reconstructions of systems with variations in density and composition. This technique has been extensively used to characterize a wide range of materials, such as rocks [10] and biological tissues [11], providing insights into porosity, vacancies, and density variations in complex systems. X-ray microtomography operates by generating images based on regions of differing density. While previous studies in

* Corresponding author.
E-mail address: aolivei@usp.br (A.O. Neto).

https://doi.org/10.1016/j.ijoes.2025.101090
Received 18 March 2025; Received in revised form 30 May 2025; Accepted 30 May 2025
Available online 31 May 2025

fields such as electrochemical systems research have applied microtomography primarily to investigate solids and electrode effects [12], this technique is far more versatile and can indeed be extended to electrochemical systems. In electrochemical cells, electrodes, electrolytes, and ionic species naturally create concentration and density gradients at the microscale, when modulate the applied energy. Furthermore, it is well known that metal nuclei strongly absorb X-rays, enabling their detection via μCT. Therefore, this technique represents a valuable tool for the in-operando 3D study of electrolyte structuring in electrochemical processes, as demonstrated in this study, where nickel electrodeposition under potentiostatic conditions was investigated using X-ray μCT.

2. Experimental

The electrochemical experiments were conducted using a three-electrode cell connected to an Ametek PARSTAT 3000A-DX bipotentiostat/galvanostat. Nickel electrodeposition was performed via potentiostatic chronoamperometry at two different potentials (-0.5 V and −1.2 V), using a titanium plate (1 cm^2) as the working electrode, a platinum counter electrode, and an Ag/AgCl (3 mol L^{-1}) reference electrode. The electrolyte solution consisted of 3 mol L^{-1} acetic acid, sodium acetate (0.1 mol L^{-1}), sodium lauryl sulfate at 10 mg L^{-1} , and 1 mol L^{-1} nickel sulfate (Sigma).

Morphological characterization of the electrodeposits was carried out using scanning electron microscopy (SEM) with a JSM-IT700HR (JEOL) equipped with a Schottky field emission electron gun. Three-dimensional tomography imaging was performed using a Bruker Sky-Scan 1275 X-ray μCT system, operating at 75 kV and 100 μA, with a step size of 0.2°. Image reconstruction was carried out using NRecon and CTVox software.

3. Results and discussion

Fig. 1a presents the chronoamperometric curves for nickel electrodeposition on titanium at potentials of −0.5 V and −1.2 V. It is observed that at −0.5 V, no appreciable electrodeposition currents are detected, only signs of electrochemical cell polarization. Conversely, at −1.2 V, a significantly higher current density is observed, indicating that massive nickel electrodeposition is effectively occurring [13].

Fig. 1b–d show scanning electron microscopy (SEM) images of the titanium samples under different conditions after immersion in an electrolyte containing 1 mol L^{-1} $NiSO_4$ for 60 minutes: without polarization, at −0.5 V, and at −1.2 V. In Fig. 1c, a small amount of deposited nickel is observed, occurring under an underpotential deposition (UPD) regime. However, in the sample subjected to potentiostatic cathodic polarization at −1.2 V (Fig. 1d), dendritic growth is also evident, which resulted from selecting a condition that promotes massive nickel deposition near the limiting current [14].

The selection of these experimental conditions was based on potentials expected to induce distinct effects: one potential (-0.5 V), where only system polarization occurs, with negligible electrodeposition and no significant mass transport; and another potential (-1.2 V), where substantial nickel deposition takes place on the electrode surface, inducing mass transport phenomena such as migration, diffusion, and convection [4,5]. Elemental mapping results from energy-dispersive x-ray spectroscopy (EDS) analysis showed nickel deposition levels of 0.06 wt% for the non-polarized sample, 0.2 wt% for −0.5 V, and 12 wt % for −1.2 V.

Fig. 2 presents the images obtained by X-ray μCT of the electrochemical system under three conditions: immersed in solution without polarization, polarized at −0.5 V, and polarized at −1.2 V. The system is reconstructed in 3D, with brighter regions indicating higher density.

For the non-polarized system (Fig. 2a), an increase in brightness is observed near the walls of the electrochemical cell and around the electrodes, the brightness level indicated the density of the medium possibly related to the structuring of Ni^{2+} ions in the electrical double layer, with a gradual decrease in density as a function of distance. Along the cell walls, a fainter brightness is noted, likely due to the interaction of ions with the glass surface, which typically exhibits a slight negative charge in aqueous solutions due to deprotonated silanol groups (SiO^-) [15]. This negative charge attracts electrolyte cations, forming a structured electrical double layer near the glass surface. The platinum and titanium electrodes, still disconnected from an external circuit, develop

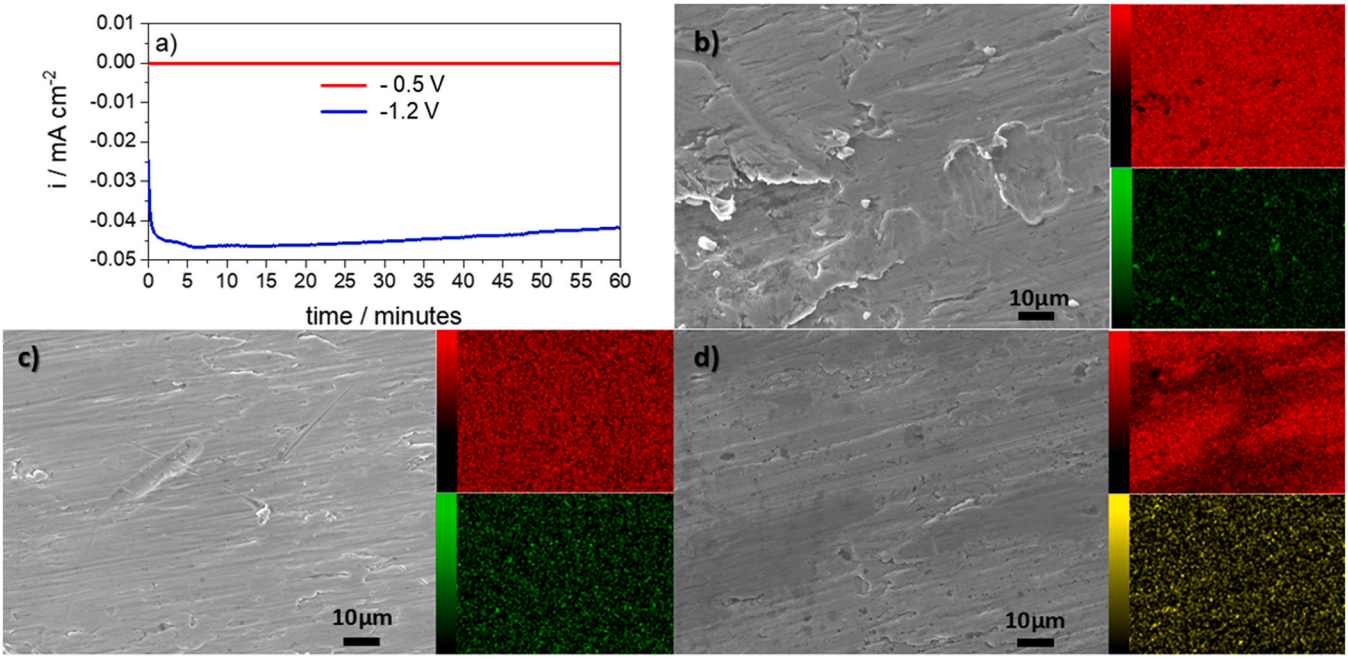

Fig. 1. a) Chronoamperometric curves for nickel electrodeposition on titanium at −0.5 V and −1.2 V vs (Ag/AgCl 3 mol L^{-1} KCL). b) SEM image elemental mapping of the titanium sample without polarization in red and Ni in green color. c) SEM image elemental mapping of the titanium sample polarized at −0.5 V in red and Ni in green color d) SEM image with elemental mapping of the titanium sample polarized at −1.2 V. in red and Ni in yellow color.

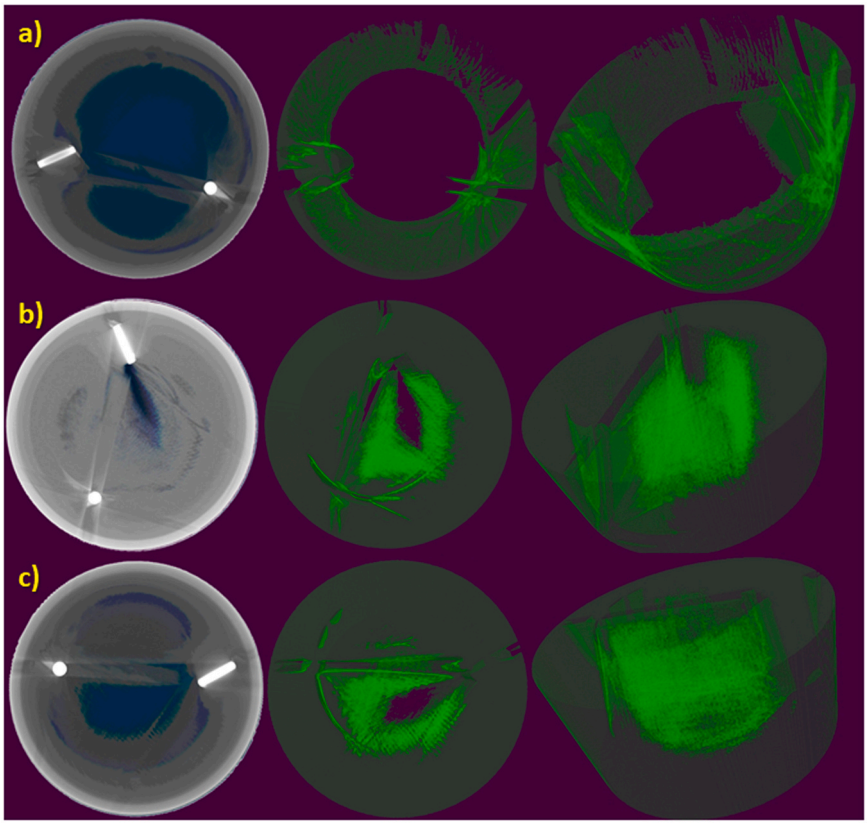

Fig. 2. Top-view and 3D reconstruction via X-ray microcomputed tomography of the electrochemical system under different polarization conditions: a) No polarization; b) Polarization at −0.5 V; and c) Polarization at −1.2 V. The grayscale figure present the position of platinum (circle) and titanium (rectangle) electrodes and images were reconstructed. In contrast, the green 3D images depict maximum opacity, reconstructed with CTAn and CTVol software, thereby highlighting the Nickel particles rendered in bright green.

their own double layers at the electrode-electrolyte interface, exhibiting a higher ionic density than that observed near the glass. The ionic distribution in this region depends on the intrinsic work function of the electrode material and the electrolyte composition. In areas farther from the interfaces, the brightness associated with Ni^{2+} ions is practically absent, likely due to the equipment's resolution limitations and the random distribution of ions in the bulk solution, which are smaller than the system's detection limit.

When a potential of −0.5 V is applied (Fig. 2b), which is insufficient for nickel electrodeposition as demonstrated in Fig. 1, it is observed that the entire space between the electrodes becomes filled with the brightness attributed to Ni^{2+} ion interactions. Previously dispersed throughout the electrochemical cell in low-density regions, these ions migrate toward the region between the polarized electrodes, forming a subtle gradient in the 3D space that appears as a diffuse cloud surrounding the electrodes.

At −1.2 V, a potential sufficient for massive nickel electrodeposition on titanium (Fig. 2c), redox reactions initiate, leading to Ni^{2+} ion consumption and altering the electrolyte structure. The rapid reduction of Ni^{2+} in the vicinity of the cathode creates a concentration gradient. The resulting mass transport by migration leads to deposition layers and depletion zones, where Ni^{2+} ions diffuse from the bulk toward the interface, establishing a diffusion layer. While the bulk solution remains globally neutral, a continuous flux of ions replenishes the consumed Ni^{2+}.

This phenomenon is evident in Fig. 2c, where bright regions and vacancies likely correspond to depletion zones. Marshall [7] theoretically describes that during electrodeposition, the 3D electrolyte structure exhibits complex concentration layers, where ions organize into depletion zones. Migration generates density gradients due to variations in concentration and temperature. Rayleigh-Bénard convection is an example of this effect[16], where less dense electrolyte rises and denser electrolyte sinks. Vortices are observed due to electrokinetic instabilities and the interaction between different transport modes. These vortices can take various forms, such as rings or counter-rotating pairs, influencing ion transport to the electrode surface (Fig. 2c).For more detailed 3D information on electrolyte structuring, the reconstructions are available as supplementary files in STL format.

4. Conclusion

This study demonstrates the potential of X-ray microcomputed tomography as a powerful tool for qualitative in-operando investigation of electrochemical systems, particularly in the electrodeposition of nickel under potentiostatic conditions. The combination of chronoamperometry, scanning electron microscopy (SEM), and X-ray μCT provided complementary insights into the deposition process, revealing key mass transport phenomena such as migration, diffusion, and convection.The X-ray μCT images allowed the visualization of ionic structuring within the electrolyte, confirming the presence of Ni^{2+} concentration gradients and depletion zones near the electrode surface. The observed dendritic growth at −1.2 V further emphasizes the influence of transport phenomena on the morphological evolution of electrodeposited layers. Moreover, the detection of ion migration and the formation of structured ionic layers near polarized electrodes reinforces the capability of X-ray μCT in capturing dynamic electrochemical interactions in three dimensions.These findings highlight the complexity of mass transport in electrodeposition processes and underscore the need for advanced characterization techniques to refine theoretical models.

CRediT authorship contribution statement

Gabriel Silvestrin: Methodology. **Lorenzo De Micheli:** Methodology. **Edson P. Soares:** Investigation. **Claudia Giovedi:** Investigation. **Wilson Calvo:** Investigation. **Rodrigo F.B. de Souza:** Writing – original draft. **Andrea S. Del Pozzo:** Investigation, Formal analysis. **Antonio D. Giuliano:** Investigation. **Terremoto Luis A. A.:** Writing – review & editing. **Samir L. Somessari:** Investigation. **oliveira neto Almir:** Funding acquisition.

Declaration of Competing Interest

The authors declare that they have no known competing financial interests or personal relationships that could have appeared to influence the work reported in this paper.

Acknowledgements

CNPq (302709/2020-7, 407967/2022), IEA - BRA1036, and FDTE for financial support.

Appendix A. Supporting information

Supplementary data associated with this article can be found in the online version at doi:10.1016/j.ijoes.2025.101090.

References

[1] C. Ramírez, B. Bozzini, J.A. Calderón, Electrodeposition of copper from triethanolamine as a complexing agent in alkaline solution, Electrochim. Acta 425 (2022) 140654, https://doi.org/10.1016/j.electacta.2022.140654.
[2] J. Ajayi-Majebi, O.P. Abioye, O.S.I. Fayomi, A.O. Inegbenebor, Review of electrodeposition perspectives towards anticorrosion mitigation of mild steel, IOP Conf. Series: Mater. Sci. Eng., 1107 (2021) 012082. ⟨10.1088/1757-899X/1107/1/012082⟩.
[3] B. Yue, G. Zhu, Y. Wang, J. Song, Z. Chang, N. Guo, M. Xu, Uncertainty analysis of factors affecting coating thickness distribution during nickel electrodeposition, J. Electroanal. Chem. 891 (2021) 115274, https://doi.org/10.1016/j.jelechem.2021.115274.
[4] Z. Ma, B. Jiang, Y. Dong, J. Qiang, D. Drummer, L. Zhang, Electrodeposition model with dynamic ion diffusion coefficients for predicting void defects in electroformed microcolumn arrays, Phys. Chem. Chem. Phys. 25 (2023) 7407–7416, https://doi.org/10.1039/D2CP05396A.
[5] A. Sharma, A. Mukherjee, A. Warren, S. Jin, G. Li, D.L. Koch, L.A. Archer, Electroconvective flow in liquid electrolytes containing oligomer additives, Langmuir 39 (2023) 92–100, https://doi.org/10.1021/acs.langmuir.2c02210.
[6] A.R. Averill, H.S. Mahmood, Forced convection mass transfer in electrodeposition cells-theoretical aspects, Trans. IMF 74 (1996) 11–16, https://doi.org/10.1080/00202967.1996.11871082.
[7] G. Marshall, E. Mocskos, F.V. Molina, S. Dengra, Three-dimensional nature of ion transport in thin-layer electrodeposition, Phys. Rev. E 68 (2003) 021607, https://doi.org/10.1103/PhysRevE.68.021607.
[8] S.V.K. Anicode, E. Madenci, N. Phan, A unified method to simulate electrodeposition and galvanic corrosion using the peridynamic differential operator, Comput. Methods Appl. Mech. Eng. 408 (2023) 115968, https://doi.org/10.1016/j.cma.2023.115968.
[9] V.S. Protsenko, F.I. Danilov, Kinetic model of composite coatings electrodeposition assuming irreversible adsorption of dispersed particles on a growing metal substrate, J. Electroanal. Chem. 918 (2022) 116463, https://doi.org/10.1016/j.jelechem.2022.116463.
[10] H. Chen, X. Cao, X. Zhang, Z. Wang, B. Qiu, K. Zheng, Automatic segmentation framework of X-Ray tomography data for multi-phase rock using Swin Transformer approach, Sci. Data 10 (2023) 812, https://doi.org/10.1038/s41597-023-02734-7.
[11] T. Shearer, R.S. Bradley, L.A. Hidalgo-Bastida, M.J. Sherratt, S.H. Cartmell, Three-dimensional visualisation of soft biological structures by X-ray computed micro-tomography, J. Cell Sci. 129 (2016) 2483–2492, https://doi.org/10.1242/jcs.179077.
[12] J.T. Lang, D. Kulkarni, C.W. Foster, Y. Huang, M.A. Sepe, S. Shimpalee, D. Y. Parkinson, I.V. Zenyuk, X-ray tomography applied to electrochemical devices and electrocatalysis, Chem. Rev. 123 (2023) 9880–9914, https://doi.org/10.1021/acs.chemrev.2c00873.
[13] M. Schlesinger, M. Paunovic, Modern Electroplating, Wiley, 2010.
[14] M. Huang, K. Skibinska, P. Zabinski, M. Wojnicki, G. Włoch, K. Eckert, G. Mutschke, On the prospects of magnetic-field-assisted electrodeposition of nanostructured ferromagnetic layers, Electrochim. Acta 420 (2022) 140422, https://doi.org/10.1016/j.electacta.2022.140422.
[15] S. Parshotam, B. Rehl, F. Busse, A. Brown, J.M. Gibbs, Influence of the hydrogen-bonding environment on vibrational coupling in the electrical double layer at the silica/aqueous interface, J. Phys. Chem. C. 126 (2022) 21734–21744, https://doi.org/10.1021/acs.jpcc.2c06412.
[16] J.C. de Valença, A. Kurniawan, R.M. Wagterveld, J.A. Wood, R.G.H. Lammertink, Influence of Rayleigh-B\'enard convection on electrokinetic instability in overlimiting current conditions, Phys. Rev. Fluids 2 (2017) 033701, https://doi.org/10.1103/PhysRevFluids.2.033701.